RESEARCH ARTICLE
SOLID EARTH: GEOELECTROMAGNETICS

Earth and Planetary Physics
9: 500–510, 2025
doi: 10.26464/epp2025024

Combining polar-orbiting and low-inclination satellites — Joint analysis of data from MSS-1 and *Swarm*

Nils Olsen*

DTU Space, Technical University of Denmark, Akademivej 356, 2800 Kongens Lyngby, Denmark

Key Points:

- Complementary roles of *Swarm*'s polar orbit and MSS-1's low-inclination orbit for geomagnetic field modelling.
- Close encounters between MSS-1 and *Swarm* (separation < 100 km) confirm the high data quality of both satellite missions.
- Joint analysis of data during the May 2024 geomagnetic storm reveals a clear dawn–dusk asymmetry of the storm-time equatorial magnetic disturbances.

Citation: Olsen, N. (2025). Combining polar-orbiting and low-inclination satellites — Joint analysis of data from MSS-1 and *Swarm*. *Earth Planet. Phys.*, *9*(3), 500–510. http://doi.org/10.26464/epp2025024

Abstract: This article investigates the combination of magnetic data from the MSS-1 and *Swarm* satellites for improved investigations of Earth's magnetic field and Geospace. The study highlights the complementary nature of polar-orbiting (*Swarm*) and low-inclination (MSS-1) satellites in geomagnetic modelling and monitoring large-scale magnetospheric contributions. Data from close encounters between MSS-1 and *Swarm* (intersatellite distance < 100 km) confirm the excellent data quality of the two satellite missions (< 1 nT median difference in scalar intensity *F*) and allow for data calibration and validation and investigations of in-situ ionospheric currents. The reason for a small but consistent difference (*F* as measured by MSS-1 is 0.5 to 1.0 nT larger than that measured by *Swarm*) is unknown. Combining MSS-1's low-inclination data with *Swarm*'s near-polar observations significantly enhances the spatial–temporal resolution of Earth's magnetic field models, allowing for new opportunities for studying both rapid core field variations at low latitudes and the local-time dependence of large-scale magnetospheric current systems. A joint analysis of magnetic data from six satellites during the May 2024 geomagnetic storm reveals a clear dawn–dusk asymmetry, with equatorial magnetic disturbances during dusk being approximately 150 nT more negative than during dawn.

Keywords: MSS-1 satellite; geomagnetic field modelling; *Swarm* satellite constellation; magnetic storms

1. Introduction

Most satellites for studying Earth's magnetic field operate from near-polar orbits. Examples include the satellites Magsat, Ørsted, CHAMP, SAC-C, and the *Swarm* satellite trio (e.g. Olsen and Kotsiaros, 2011; Olsen and Floberghagen, 2018). While these satellites vary slightly in their orbital inclination and Local Time coverage, their orbital inclination is above $i = 85°$, allowing them to sample the magnetic field along a predominantly North–South trajectory.

In contrast, MSS-1 (Zhang K, 2023) stands out as the first high-precision and accuracy geomagnetic satellite mission operating at a low orbital inclination of $i = 41°$. This unique orbit enables MSS-1 to sample Earth's magnetic field along trajectories with a strong East–West component. In addition, the low-inclination orbit leads to a space-time sampling pattern very different from those of near-polar orbiting satellites. When selecting data for geomagnetic field modelling, it is essential to understand the peculiarities of satellites in near-polar and low-inclination orbits. This is the topic of Section 2. The orbital path of MSS-1 leads to frequent "close encounters" with the *Swarm* satellites; investigation of these encounters will be discussed in Section 3. Section 4 deals with modelling the space–time structure of large-scale magnetospheric contributions by a joint analysis of simultaneous magnetic field observations from MSS-1, *Swarm* and other satellites. The paper concludes with a summary of the findings and possible future perspectives in Section 5.

2. Satellites in Near-polar vs. Low-inclination Orbits

A proper global sampling of the entire Earth is only possible with exactly polar-orbiting satellites ($i = 90°$). Since only latitudes up to $\pm i$ are visited, even near-polar orbiting satellites like *Swarm* never sample the regions around the geographic poles with angular radius $90° - i$, which, for example for *Swarm* Bravo (also denoted as *Swarm* B, $i = 88.0°$) corresponds to spherical caps of radius 2.0° (roughly 220 km). These unsampled regions — one centred on the Northern and the other on the Southern geographic pole — will be denoted as "primary polar gaps" since they only depend on the satellite's orbital inclination and thus do only weakly, if at all, change with time.

Correspondence to: N. Olsen, nio@space.dtu.dk
Received 20 DEC 2024; Accepted 05 FEB 2025.
First Published online 05 MAR 2025.

When estimating models of Earth's magnetic field, there is another cause of gaps in data sampling: During the selection of magnetic data for geomagnetic field modelling, one typically excludes data from regions exposed to solar irradiation to minimise the influence of magnetic disturbances from ionospheric currents. Ionospheric E-layer conductivity during geomagnetic quiet conditions and at non-polar latitudes is mainly caused by solar EUV radiation, and the magnetic disturbances of ionospheric currents are minimised by selecting data from dark regions. A commonly used criterion is that the Sun has to be at least 10° below the horizon (i.e. solar elevation angle $\eta < -10°$) as introduced by Olsen (2002). Due to the tilt of Earth's rotation axis with respect to the Sun–Earth connection line and its seasonal variation, the regions centred at the poles not fulfilling the criteria $\eta < -10°$ have an angular radius of up to 33°. For polar-orbiting satellites like *Swarm*, a data selection according to the "dark" criteria implies data gaps of several months in the polar regions, which severely hampers the determination of rapid core field changes. In the following, I will call these regions "seasonal polar gaps" since they only exist during the summer months in the respective hemisphere.

Let us first look at the near-polar orbiting satellite *Swarm* Bravo. The green dots in Figure 1 show the distribution of its "dark" data for three one-week long periods in May 2024 sampled every minute (here I only select data according to solar elevation angle $\eta < -10°$; any additional data selection on geomagnetic activity will further decrease the number of data although likely not in a systematic way regarding geographic coverage). The "dark" selection criterion removes all data above ≈ +65° geographic latitude, leaving a large data gap around the geographic North Pole. As expected when approaching solstice conditions, this gap becomes larger towards the end of May.

Focusing on the distribution in latitude and time, the upper part of Figure 2 shows the seasonal dependency of this "dark" selection criteria; grey represents the latitude and time where Sun elevation angle $\eta > -10°$ even during local midnight, i.e. when the "dark" criteria can not be fulfilled regardless of the Local Time of the satellite. The red and green areas show periods for which this criteria is fulfilled for *Swarm* Alpha and Bravo, respectively; brown colours indicate areas with the criteria fulfilled for both *Swarm* Alpha and Bravo.

The Local Time of the satellite's equator crossings is shown in the middle panel of Figure 2; the solid line represents LTAN (*Local Time of the Ascending Node*, i.e. that of the northbound equator crossings) and the dashed line being Local Time of the descending (southbound) node. A satellite in a dawn–dusk orbit during equinoxes will not be able to fulfil the dark-criteria at any latitude (see e.g. the gap in *Swarm* Bravo data around October 2023), while the criteria may be fulfilled for some latitudes for a dawn–dusk orbit configuration during solstices.

Let us now move to the low-inclination orbiting satellite MSS-1 (i = 41°), for which the situation is rather different compared to *Swarm*. The "primary polar gap" is, of course, much larger since regions poleward of ±41° latitude are not visited by MSS-1. This also implies that the "seasonal polar gap" (which for polar-orbiting satellites is typically much larger than their "primary polar gap") has only very limited, if any, influence for MSS-1. However, the fast orbital drift of MSS-1 and the rapid change in Local Time leads to yet another unsampled region when selecting data from "dark" areas: such data are only available in one hemisphere for about three weeks, while three weeks later only the other hemisphere is sampled during dark conditions.

This is shown in Figure 1: MSS-1 "dark" data (blue dots) are only available for southern latitudes during the first week of May 2024, while only northern latitudes are available at the end of that month. LTAN of MSS-1 sweeps over all local times (0 to 24 hours) in 52 days, and combining southbound and northbound parts of each orbit implies that MSS-1 samples all local times in 26 days. These rapid changes in the latitudes of "dark" regions visited by MSS-1 are also seen in the top panel of Figure 2.

What is the impact of these data selection criteria on geomagnetic

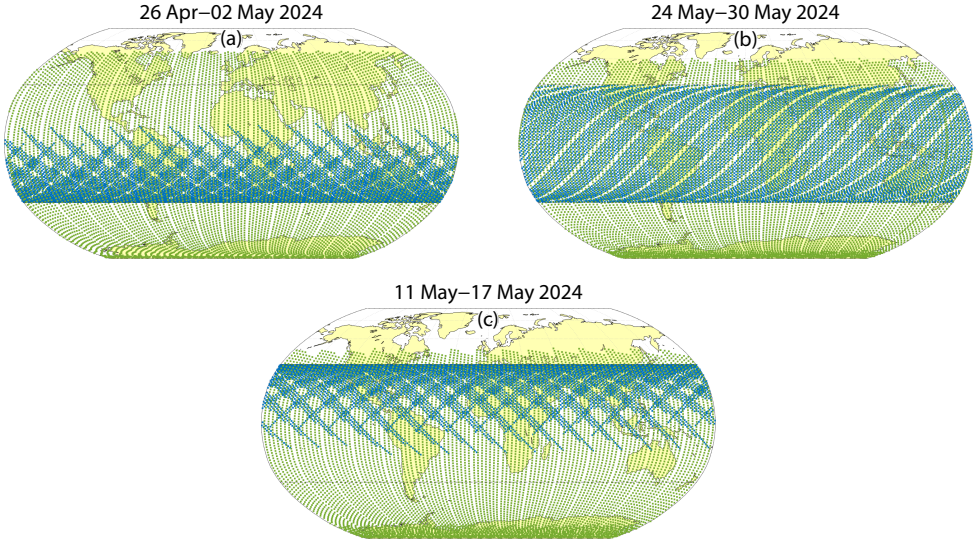

Figure 1. Availability of "dark" 1-minute data provided by *Swarm* Bravo (green dots) and MSS-1 (blue dots), respectively, for one week at the beginning of May 2024 (a), in mid-May (b), and at the end of May 2024 (c).

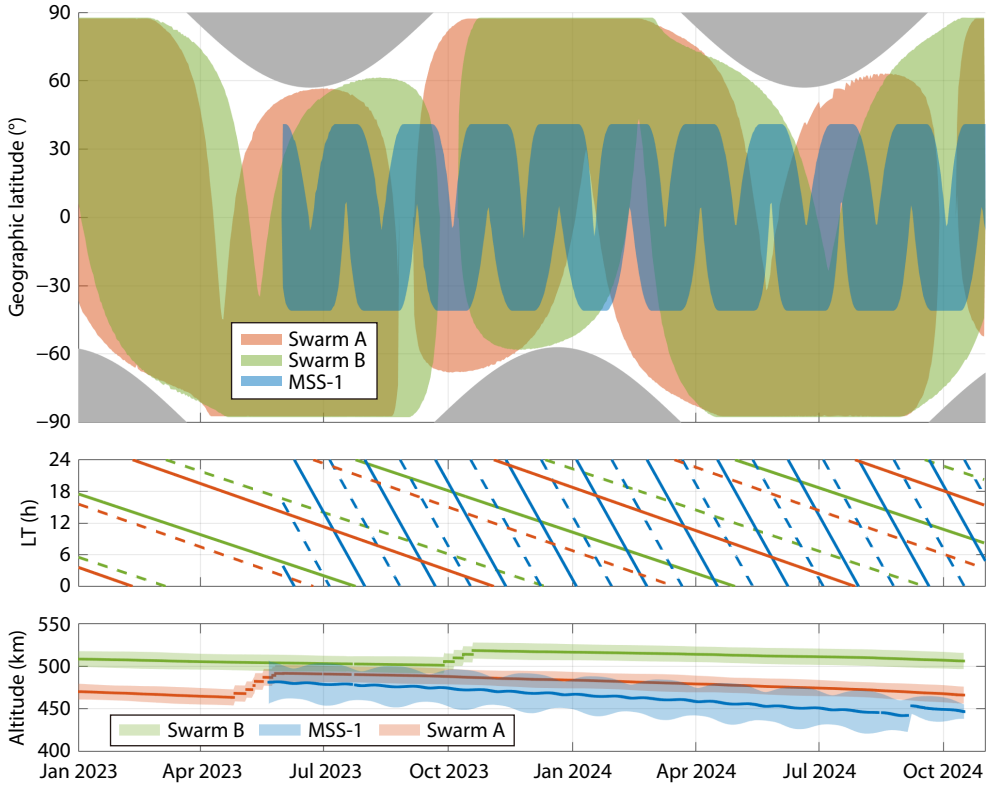

Figure 2. Top: Availability of "dark" *Swarm* Alpha (red), *Swarm* Bravo (green) and MSS-1 (blue) satellite data as a function of geographic latitude and time. The grey patches illustrate latitude regions when the "dark" criteria (Sun at least 10° below the horizon) are not fulfilled. Middle: Local Time of northbound (solid lines) and southbound (dashed lines) equatorial crossing for *Swarm* Alpha, (red), *Swarm* Bravo (green) and MSS-1 (blue), respectively. Bottom: Satellite altitude above a mean Earth radius of a = 6371.2 km.

field modelling? When using data spanning at least one year, only the "primary polar gap" of near-polar orbiting satellites — no data are available at latitudes poleward of $\pm i$ — is of concern for the determination of lithospheric expansion coefficients of high spherical harmonic degree n and low order m. Since only Legendre functions of order $m = 0$ are non-zero at the poles, missing data close to the poles mainly affect the zonal ($m = 0$) spherical harmonic expansion coefficients. Experience with CHAMP (i = 87.3°) and *Swarm* (i = 87.4° to 88.0°) have shown that their "primary polar gap" only affects expansion coefficients of degree above n = 60 (Olsen et al., 2014) which can be handled e.g. by model regularisation.

However, when studying temporal variations of Earth's magnetic field the impact of the dark selection criteria has to be noted. The lack of high-latitude satellite data severely hampers the determination of rapid core field changes during summer. This, again, mainly affects polar regions and thus the zonal ($m = 0$) and near-zonal (small m) spherical harmonic coefficients. In contrast, low-latitude features are primarily described by near-tesseral coefficients ($m \approx n$); therefore, the time changes of near-tesseral coefficients are likely better determined than those of the near-zonal coefficients ($m \approx 0$).

Although it is not possible to determine global geomagnetic field models solely using data from low-inclination satellites like MSS-1, one of the advantages of low-inclination satellites is their denser data sampling at low latitudes and that they span all local times at all latitudes between $\pm i$ within a few weeks. This is, for instance, advantageous for the determination of low-latitude "Geomagnetic Virtual Observatories in Space", GVOs (Mandea and Olsen, 2006; Hammer et al., 2021): To minimise disturbances from ionospheric currents and to avoid a bias introduced by selecting data taken for specific local times it is preferable to include data from a time segment long enough such that the satellite has sampled all local times; for *Swarm* this corresponds to 4 months. 4-monthly *Swarm* GVOs are therefore less affected by external magnetic field disturbances compared to a 1-monthly version, as demonstrated by Hammer et al. (2021). The much faster orbital drift of MSS-1 allows this period to be shortened from 4 months to 26 days, and thus GVOs determined from MSS-1 magnetic data are expected to be particularly useful for studying rapid core field changes at low latitudes.

3. Close Encounters Between MSS-1 and *Swarm*

The different orbital inclinations of MSS-1 and the *Swarm* satellites result in frequent "close encounters" between two or more satellites. In the following, I consider a "close encounter" when the inter-satellite distance is below 100 km. This can only happen when the Local Time of the satellites agree within a few minutes (a Local Time difference of 4 minutes corresponds to a 1° longitudinal difference, which transforms to about 111 km near the equator). Looking at the middle panel of Figure 2, close encounters between MSS-1 and *Swarm* are therefore possible for any combination of northbound (solid lines) and southbound (dashed lines)

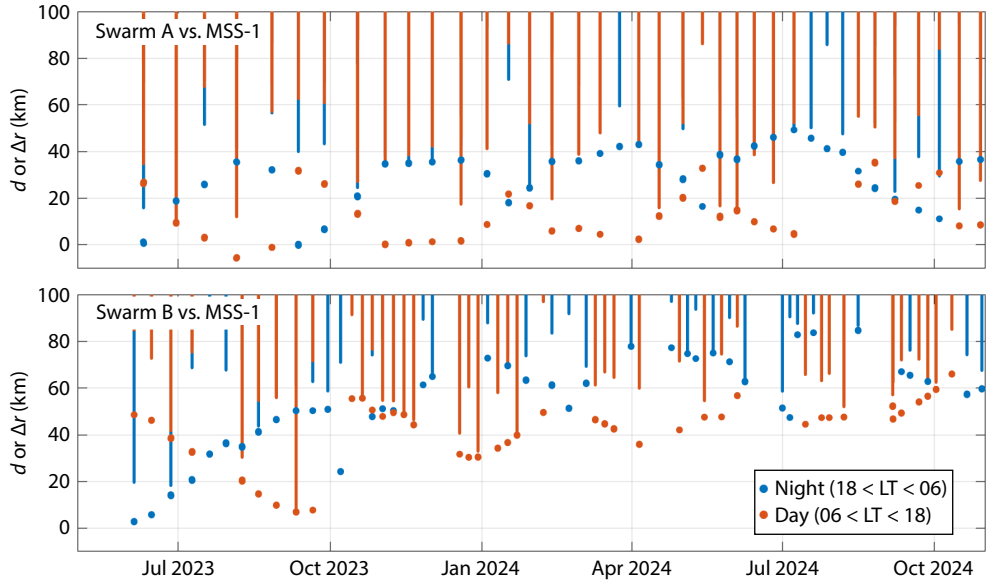

Figure 3. Close encounters between MSS-1 and *Swarm* Alpha (top), respectively *Swarm* Bravo (bottom). The solid lines show the inter-satellite distance d for encounters during nighttime (blue) and daytime (red), respectively, while the dots represent the corresponding altitude difference Δr (negative if MSS-1 is above *Swarm*).

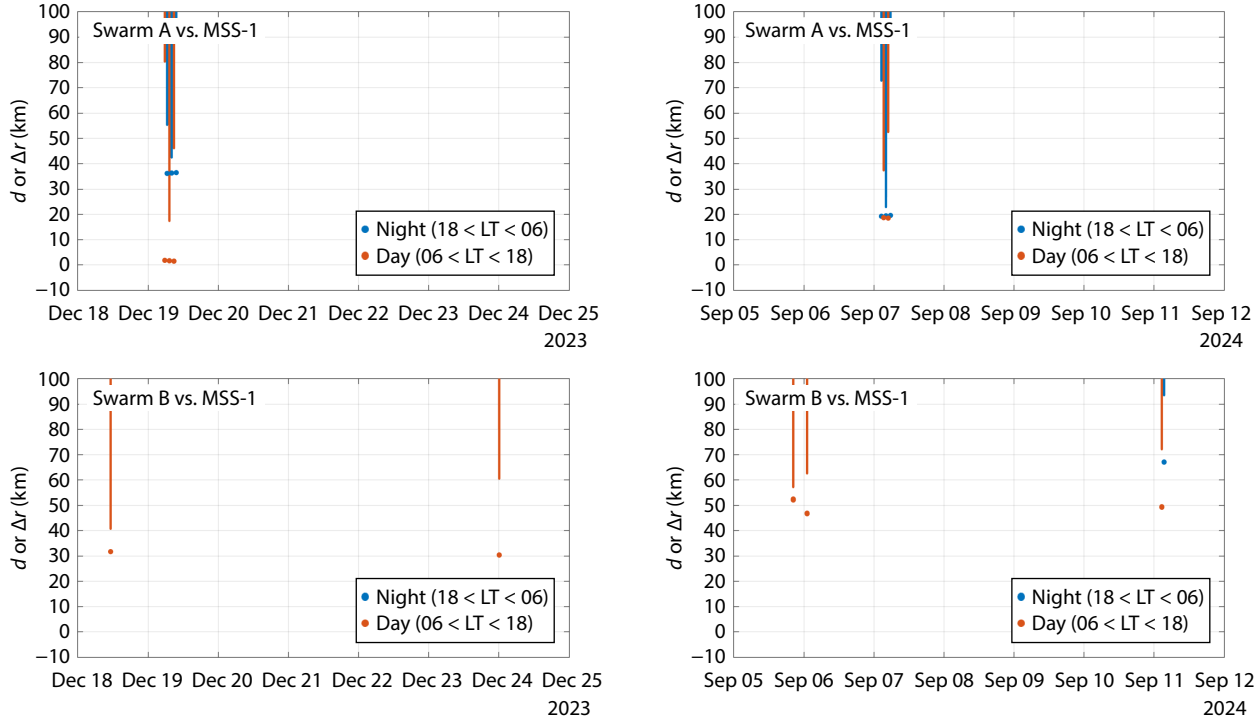

Figure 4. Similar to Figure 3 but for one week in December 2023 (left) and September 2024 (right), respectively.

equatorial crossings, which typically happens approximately every 2 to 3 weeks for MSS-1 and *Swarm* A. The top panel of Figure 3 shows the time instants of these close encounters, i.e. when the distance d between MSS-1 and *Swarm* Alpha is below 100 km. Due to changing orbital configuration, close encounters occur more frequently (about every 10th day) towards the end of the period in consideration, compared to the situation in summer 2023 (about every 18th day).

The lower part of Figure 3 shows close encounters between MSS-1 and *Swarm* B; also these occur more frequently towards the end of the considered period (about every 5th day).

Most close encounters between MSS-1 and *Swarm* occur in groups rather than as single events. This is illustrated in Figure 4 for two periods in December 2023 (left) and September 2024 (right), respectively. There are five encounters closer than 100 km with *Swarm* Alpha on 19 December 2023 (top left) and five on 7 September 2024 (top right), occurring alternately on the dayside (red) and nightside (blue) and approximately separated by 45

minutes (i.e. half of the orbital period). The situation is similar for encounters between MSS-1 and *Swarm* Charlie because of the similar orbit of the latter with *Swarm* Alpha.

There are no such groups of close encounters between MSS-1 and *Swarm* Bravo. The close encounters occur more often, as illustrated in the lower part of Figure 4 but there are fewer than between MSS-1 and *Swarm* Alpha due to the larger altitude difference of their orbits.

Close encounters provide a unique possibility not only for inter-satellite data calibration and validation but also for investigations of in-situ ionospheric currents. In the following, I look at the statistics of the magnetic field differences sampled at 1 Hz during 198 close encounters between MSS-1 and *Swarm* (73 encounters with *Swarm* Alpha, 56 with Bravo, and 69 with Charlie) for the 13 months starting in November 2023. The duration of these close encounters is between 4 and 30 seconds with an average of 13 seconds.

The left part of Figure 5 shows the difference $\Delta F = \delta F_{\text{MSS-1}} - \delta F_{\text{SW}}$ of the scalar intensity measurements between MSS-1 and each of the three *Swarm* satellites as a function of inter-satellite distance d. Here $\delta F = F^{\text{obs}} - F^{\text{mod}}$ is, for each satellite, the difference between observations F^{obs} and model values F^{mod} of the core, lithospheric and magnetospheric field as given by the CHAOS-7 model of Finlay et al. (2020). Blue curves correspond to nighttime data (Local Time between 18 and 06) while red curves represent daytime data. The right part of the figure shows the corresponding normalised histograms (i.e. estimates of probability density func-

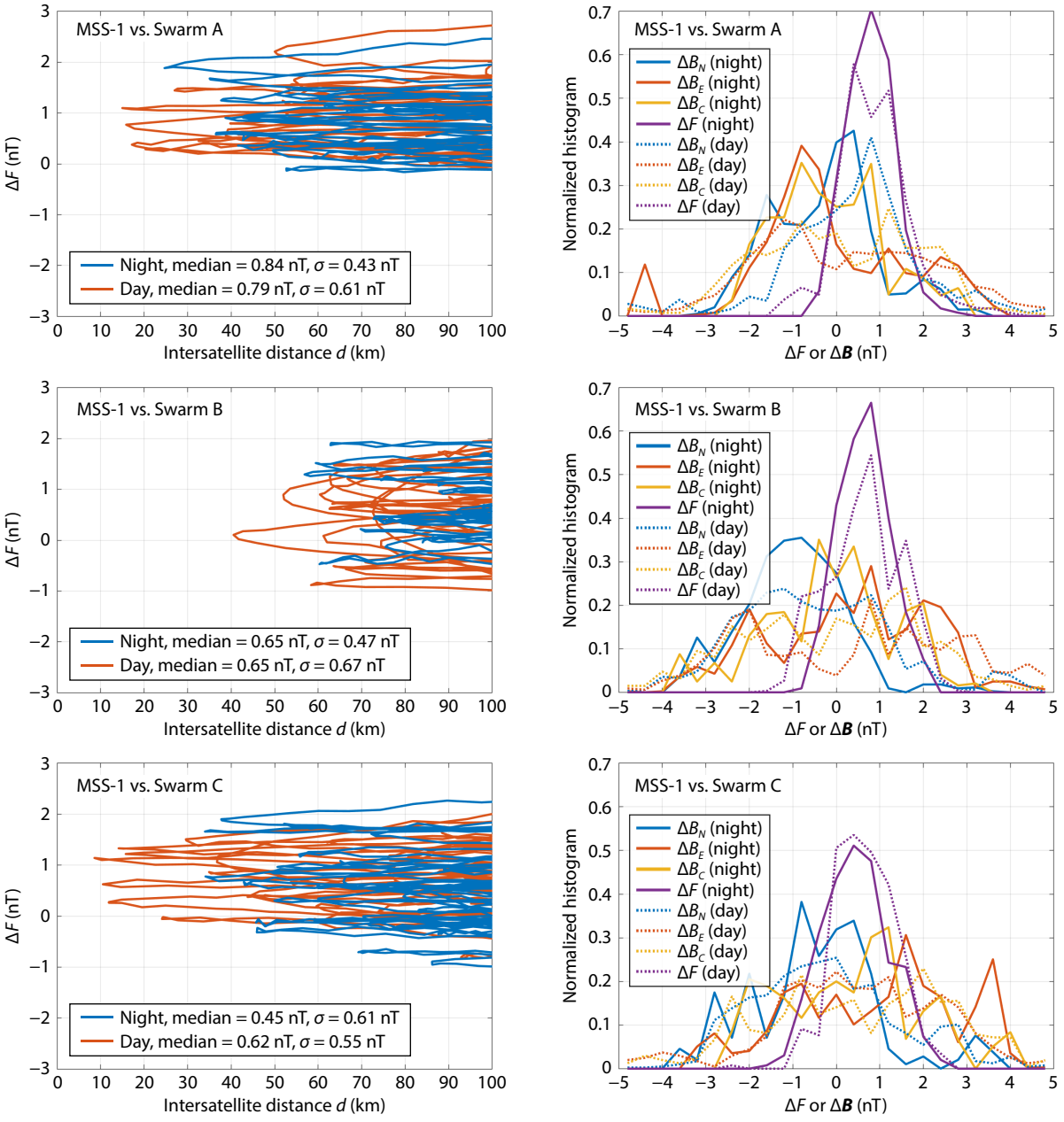

Figure 5. Left: Difference in magnetic field intensity, ΔF, between MSS-1 and each of the *Swarm* satellites as a function of inter-satellite distance d. Right: Normalised histogram of the difference in scalar intensity ΔF and in the three vector components $\Delta \boldsymbol{B}_{\text{NEC}}$.

Table 1. Median and MAD (in nT) and number of data points N_{data} of the close encounters between MSS-1 and each of the three *Swarm* satellites between November 2023 and November 2024.

		Swarm Alpha			*Swarm* Bravo			*Swarm* Charlie		
		N_{data}	median	σ (MAD)	N_{data}	median	σ (MAD)	N_{data}	median	σ (MAD)
Night	ΔB_N	426	−0.25	1.01	272	−0.69	1.08	460	−0.64	1.10
	ΔB_E	426	−0.39	1.31	272	0.63	1.56	460	0.94	1.62
	ΔB_C	426	−0.17	1.02	272	−0.24	1.15	460	0.21	1.29
	ΔF	426	0.85	0.45	272	0.52	0.58	460	0.55	0.59
Day	ΔB_N	400	0.52	0.94	277	−0.53	1.31	401	−0.56	1.10
	ΔB_E	400	0.15	1.78	277	0.96	2.80	401	0.54	1.48
	ΔB_C	400	−0.01	1.54	277	0.16	1.75	401	0.17	1.80
	ΔF	400	0.72	0.49	277	0.67	0.61	401	0.74	0.50
All	ΔB_N	826	0.07	1.03	549	−0.65	1.18	861	−0.57	1.09
	ΔB_E	826	−0.24	1.54	549	0.73	2.19	861	0.74	1.56
	ΔB_C	826	−0.04	1.27	549	−0.06	1.46	861	0.19	1.52
	ΔF	826	0.79	0.47	549	0.59	0.59	861	0.59	0.55

tions) for ΔF and the vector components $\Delta \boldsymbol{B}_{NEC}$ in the North, East and Center (NEC) coordinate frame. Median and Mean Absolute Deviation (MAD) of ΔF and $\Delta \boldsymbol{B}_{NEC}$ as well as the number of data points N_{data} used in their determination are listed in Table 1.

Several aspects are interesting to notice: Firstly, there is remarkably good agreement between the magnetic field measured by MSS-1 and each of the *Swarm* satellites. Despite the different platform designs and instruments, most differences in ΔF during individual close encounters are very small (left part of Figure 5). They scatter by less than 1 nT (σ between 0.52 and 0.85 nT) around their median values (0.47 to 0.87 nT, see Table 1). This convincingly demonstrates the high quality of the magnetic data collected by the two satellite missions. Secondly, ΔF depends only weakly on the inter-satellite distance d, which speaks against a geophysical cause of the difference. Thirdly, there is hardly any difference between dayside and nightside data, and thus the impact of in-situ ionospheric currents at satellite altitude appears minimal, at least for the scenarios considered here. And finally, there is a consistent, although small, difference in scalar intensity F as measured by MSS-1 and *Swarm* for the individual close encounters: most of the values of ΔF are *positive*, i.e. the scalar intensity measured by MSS-1 is seemingly slightly higher (0.66 nT when averaging over all three satellites and considering day and night data) than that observed by *Swarm*.

The differences in the magnetic vector components, $\Delta \boldsymbol{B}_{NEC}$, between MSS-1 and *Swarm* during close encounters are larger than those in scalar intensity ΔF, as shown by the numbers in Table 1. The scatter, expressed by the MAD, is not only larger in the vector components (1.0 to 2.8 nT) compared to scalar intensity (0.45 to 0.61 nT) but there is also less consistency in terms of the median value compared to the always positive values of ΔF. Calibration and alignment of magnetic vector components $\boldsymbol{B}_{NEC}$ requires, in addition to magnetometer readings, also attitude data. This is not the case for scalar magnetic intensity F and could be the reason for the larger difference in $\Delta \boldsymbol{B}_{NEC}$ compared to ΔF. However, the cause of the particularly large scatter in the magnetic East-component ΔB_E is not known.

To conclude: there is excellent agreement between the magnetic field measurements of MSS-1 and the *Swarm* satellites, as demonstrated by the low median difference (< 1 nT) during close encounters. But still, there seem to be some consistent differences, for instance a slightly larger (by 0.5 to 1.0 nT) magnetic field intensity measured by MSS-1. Data from the presently available close encounters do not allow for drawing sound conclusions on the reason for these differences, and future data will hopefully help to further improve the high quality of the magnetic data from both missions further.

4. Magnetospheric Currents Monitored by a Joint Analysis of MSS-1 and *Swarm*

Let us finally combine magnetic data from MSS-1, *Swarm* and other satellites to determine the space-time structure of large-scale magnetospheric magnetic field contributions.

The map presented in Figure 1 reveals that satellites in Low-Earth Orbit (LEO) provide a fairly complete sampling in latitude and longitude, which is advantageous for modelling Earth's core and lithospheric magnetic field since they are fixed with respect to Earth. However, contributions due to ionospheric and magnetospheric current systems are mostly fixed with respect to the position of the Sun, and data distribution in such a Sun-fixed frame is rather different from that in an Earth-fixed frame.

As an example, the left part of Figure 6 shows the spatial distribution of 1-minute data from *Swarm* Alpha (red) and Bravo (green) and MSS-1 (blue) in the Earth-fixed dipole latitude / longitude frame during the four days 10–13 May 2024. This period is of special interest since it covers one of the largest geomagnetic storms of the last decades, the "Mothers Day geomagnetic storm" that started on 10 May. This event has been extensively studied

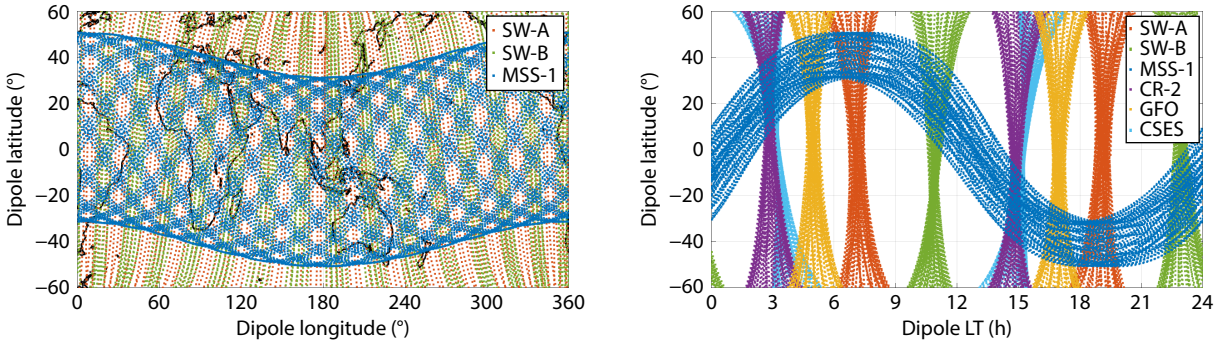

Figure 6. Left: Dipole latitude / longitude distribution of *Swarm* Alpha+Bravo and MSS-1 for the 4 days 10–13 May 2024. Right: Dipole latitude / LT distribution of six LEO satellites during those days. Only dipole latitudes between ±60° are shown.

and described; overview articles include Kwak et al. (2024); Gonzalez-Esparza et al. (2024), and Hayakawa et al. (2025). Here, I focus on the magnetic field disturbances of this event as seen by LEO satellites. The *Swarm* satellites Alpha and Bravo provide a very dense distribution in latitude and longitude; that of MSS-1 is, of course, limited to lower latitudes.

Replacing dipole longitude with dipole Local Time T_d (see Equation (14) of Hulot et al., 2015) leads to a rather different picture, as shown in the right part of the figure: dipole Local Time of *Swarm* Alpha was about 07/19 hours (similar for Charlie) and 10/22 hours for *Swarm* Bravo, which implies that neither post-midnight (T_d between 00 and 07) nor post-noon hours (T_d between 12 and 19) were sampled by *Swarm*. These gaps can be filled by magnetic data from other polar-orbiting satellites, including magnetic field intensity data from CSES and vector field "platform magnetometer data" from CryoSat-2 (CR-2, Olsen et al., 2020) and GRACE-FO (GFO, Stolle et al., 2021). However, the low-inclination MSS-1 satellite is of particular value since it samples all local times during that period, though not at all latitudes.

Combining *Swarm* and MSS-1 data for monitoring the time–space structure of large-scale magnetospheric field results in a significantly improved description compared to results obtained with *Swarm* alone.

To demonstrate this, I simulate a spherical harmonic analysis using real satellite positions for one year from 1 November 2023 to 31 October 2024, using data from all local times and assuming that contributions from the core, lithosphere and ionosphere have been removed. Thus, only the magnetic fields of magnetospheric origin and its Earth-induced counterpart are left. They are described by a scalar potential which is expanded according to

$$V = a\sum_{n=1}^{N}\sum_{m=0}^{n}\left(g_n^m(t)\cos mT_d + h_n^m(t)\sin mT_d\right)\left(\frac{a}{r}\right)^{n+1}P_n^m(\cos\theta_d) + a\sum_{n=1}^{N}\sum_{m=0}^{n}\left(q_n^m(t)\cos mT_d + s_n^m(t)\sin mT_d\right)\left(\frac{r}{a}\right)^{n}P_n^m(\cos\theta_d), \quad (1)$$

where r is radius, a = 6371.2 km is a reference Earth radius and P_n^m are the Schmidt semi-normalized associated Legendre functions of degree n and order m. N is the maximum degree and order of the expansion, θ_d is dipole co-latitude, and T_d is dipole Local Time. The coefficients $\{q_n^m, s_n^m\}$ describe external, magnetospheric, contributions, while $\{g_n^m, h_n^m\}$ describe internal contributions due to secondary, induced, currents in Earth's mantle. Collecting these coefficients in the model vector $\boldsymbol{m}$ and the measured magnetic vector components (after removal of contributions from the core and lithosphere and rotation to the dipole frame) in the data vector $\boldsymbol{d}$, the relationship between model and data vector is given by the linear relationship $\boldsymbol{d} = \boldsymbol{G}\boldsymbol{m}$. The design matrix $\boldsymbol{G}$ contains information on the satellite position and time but does not include magnetic data. To account for temporal changes of the magnetospheric and induced fields, I perform the spherical harmonic analysis in bins of length Δt and assess the stability of the solution from the condition number of the design matrix $\boldsymbol{G}$ (The condition number of a matrix is defined as the ratio of its largest to its smallest singular value). A robust determination of the coefficients requires a well-conditioned $\boldsymbol{G}$; the lower its condition number, the more stable the solution.

I determine the condition number of $\boldsymbol{G}$ for each bin of length Δt = 90 minutes (which roughly corresponds to one orbital period of LEO satellites), for a maximum spherical harmonic degree N = 2 (resulting in $2 \times N(N+2) = 16$ expansion coefficients per bin), and when using only data from *Swarm* Alpha and Bravo, respectively including MSS-1 data. The data sampling rate is 30 seconds, which means that, for each of the satellites, approximately 180 vector triplets have been used in each 90-minute bin.

The results are shown in the upper part of Figure 7. Starting with the *Swarm*-only solution (blue), there is a decrease of condition number from 4.5 in June 2023 to 2.6 in October 2024. This can be explained by the increasing separation of Local Time between *Swarm* Alpha/Charlie and *Swarm* Bravo from 2.6 hours on 1 June 2023 to 4.8 hours on 1 November 2024. The condition number is expected to decrease further until summer 2025 when the LT difference will be 6 hours, corresponding to orthogonal orbital planes. The condition number during that time will likely be similar to the value of 2.1 found during the previous 6-hour LT difference in December 2017.

However, determination of expansion coefficients up to spherical harmonic degree N = 2 from *Swarm* data alone will probably not be possible for periods of co-rotating orbital planes, as was the case in October 2021 and is expected to occur again in summer 2029. The simulation reveals a large increase of the condition number from values below 6 (when the LT difference between *Swarm* Alpha/Charlie and Bravo is larger than 2 hours) to values

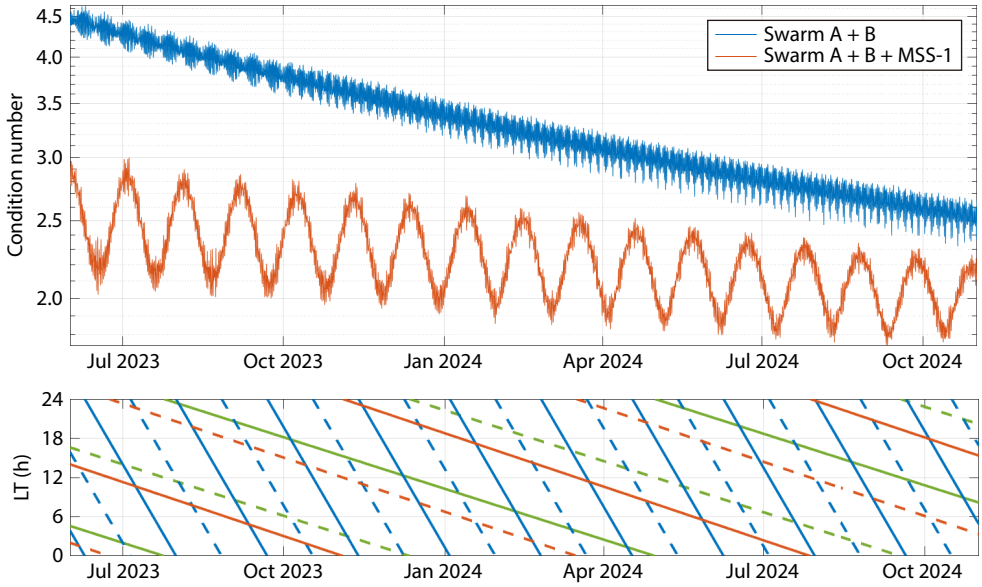

Figure 7. Top: Condition number of design matrix $\boldsymbol{G}$ for maximum spherical harmonic degree $N = 2$ and $\Delta t = 90$ minutes time segments when using only data from *Swarm* (blue) and *Swarm* plus MSS-1 (red), respectively. Bottom: Local Time of northbound (solid lines) and southbound (dashed lines) equatorial crossing for *Swarm* Alpha (red), *Swarm* Bravo (green) and MSS-1 (blue), respectively.

above 30 in October 2021 (coplanar orbits). However, including MSS-1 data considerably improves the robustness of the solution, not only for periods when all *Swarm* satellites are in similar orbital planes. This is seen by the reduction of the condition number in Figure 7 for the one year considered here. A simulation for periods of coplanar *Swarm* satellite orbits (not shown here, combining *Swarm* positions for October 2021 and synthetic MSS-1 positions for October 2023) results in a condition number below 4 when including MSS-1 data, compared to the *Swarm*-only value of ≈30, demonstrating the large benefit of combining MSS-1 and *Swarm* data.

The periodicity in the condition number seen in Figure 7 of ≈32.5 days when including MSS-1 data originates from periods when the Local Time of near-equatorial MSS-1 data is similar to those of *Swarm*. Consequently, this periodicity will vanish when the orbital planes of *Swarm* Alpha/Charlie are orthogonal to that of *Bravo* but will be largest when they are coplanar.

A small condition number of the matrix $\boldsymbol{G}$ indicates that all spherical harmonic coefficients are well determined and that the derived model is valid globally. However, a large condition number does not necessarily lead to a useless solution: if the large condition number is caused by only a few singular values of $\boldsymbol{G}$ being small (i.e. only a *combination* of spherical harmonic coefficients can be resolved) the obtained model, although not valid globally, may still be acceptable for certain regions of Earth. It is, therefore, worthwhile to derive global maps of uncertainties of the estimated magnetospheric and induced field determined

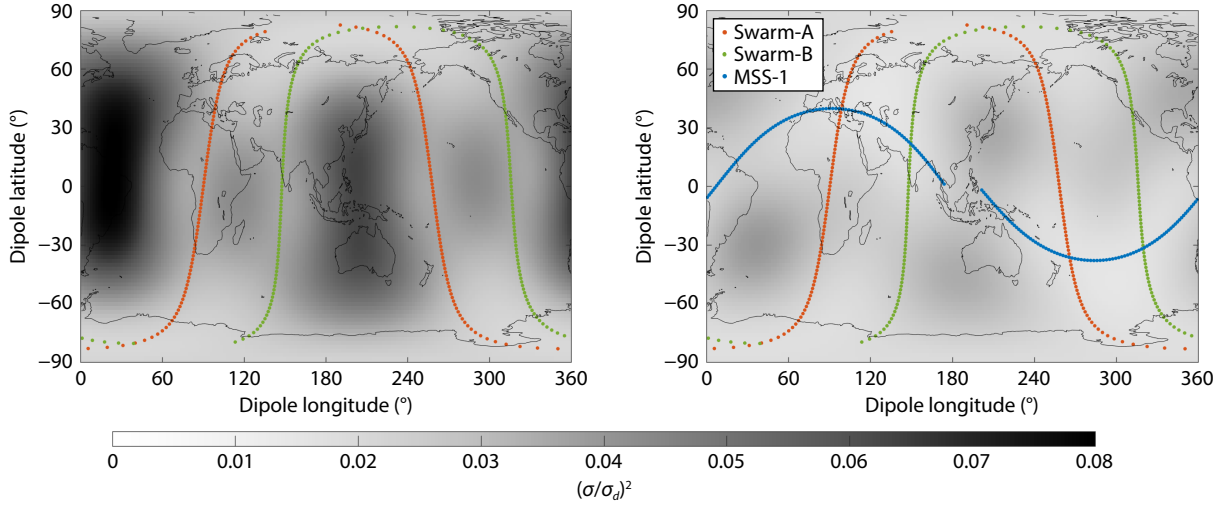

Figure 8. Map of radial magnetic component variance σ^2 (normalised by data variance σ_d^2) of magnetospheric and induced sources at Earth's surface for the 90-minute segment starting on 6 May 2024 at 18:00 UT. Left: Using only data from *Swarm* Alpha and Bravo. Right: Using also data from MSS-1.

from various spatial distributions of satellite observations.

To this aim, I follow the approach outlined in Olsen (2022) and determine the variance σ^2 of the radial component at Earth's surface, assuming uncorrelated measurement variances of amplitude σ_d^2. As an example, Figure 8 shows maps of the variance of the radial magnetic field component for the 90-minute period starting on 6 May 2024 at 18:00 UT. Its left panel shows the result when using only *Swarm* observations, while the right panel shows the corresponding map if data from MSS-1 are included. During this 90-minute segment, the *Swarm* satellites did not sample dipole longitudes around 30° and 210°, which is the reason for the increased variance around these longitudes (left panel). Adding MSS-1 data significantly reduces the uncertainties in those regions (right panel).

While these maps indicate regions where model predictions are better constrained by the data, the absolute values of the variances should be taken with care since the underlying assumption of uncorrelated data errors is highly simplified. However, experiments show that condition numbers below 4 likely lead to a robust determination of degree-2 spherical harmonic coefficients.

Is it possible to determine magnetospheric coefficients of spherical harmonic degree $N = 3$ and higher from LEO satellite data? While a robust determination is hardly possible with *Swarm* satellite data alone, and not even when including MSS-1 data — the corresponding condition numbers are well above 30 in both cases —, the inclusion of magnetic data from different Local Time sectors allows it. The ground observatory network (e.g. from INTERMAGNET) and other LEO satellites can provide such additional data. The right part of Figure 6 illustrates how magnetic data from CryoSat-2 (Olsen et al., 2020), GRACE-FO (Stolle et al., 2021) and CSES (Yang YY et al., 2021) nicely fill the Local Time gaps left by the *Swarm* mission.

To illustrate the higher spatial resolution provided by combining data from many satellites, the upper part of Figure 9 shows the near-equatorial (< ±10° dipole latitude) horizontal magnetic component ΔH measured by the various satellites, after subtraction of the core and crustal field contributions as given by the CHAOS-7 field model of Finlay et al. (2020). Each of the 6 satellites crosses the equator twice during its about 90-minute long orbit, separated by 12 hours in local time. The strongest magnetospheric current system during geomagnetic storms is arguably that of the

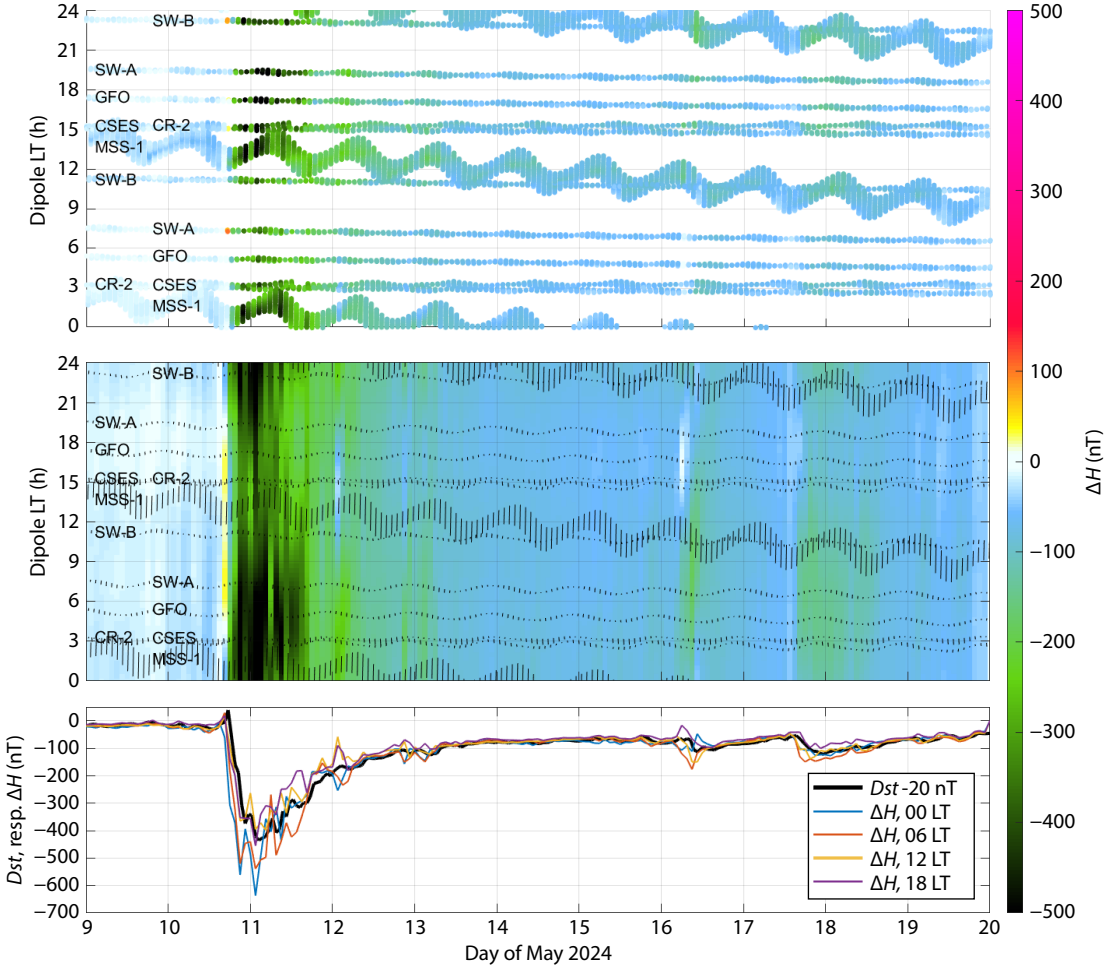

Figure 9. Top: Low-latitude (< ±10° dipole latitude) horizontal magnetic field variation ΔH for May 2024 as observed by six LEO satellites (SW-A: *Swarm* Alpha, SW-B: *Swarm* Bravo, GFO: GRACE-FO, CR-2: CryoSat-2). Middle: Horizontal magnetic field variation ΔH at the dipole equator, synthesised from a spherical harmonic expansion up to degree $N = 3$ of the magnetic data from these six satellites. Bottom: *Dst*-index of geomagnetic storm activity (black) and synthesised ΔH for various dipole Local Times.

magnetospheric ring-current, which produces a southward-directed magnetic field disturbance at the equator, corresponding to a negative variation of the horizontal component ΔH. This is obvious when comparing the time changes of the satellite observation in the top panel with those of the *Dst*-index shown in the bottom panel of the figure. *Dst* is a ground-based index that monitors geomagnetic storms.

Using the data from the six satellites under consideration, I performed a spherical harmonic expansion up to degree and order $N = 3$ in bins of length $\Delta t = 90$ minutes. From the estimated expansion coefficients time series of the horizontal magnetic field disturbance at 0° dipole latitude as a function of Local Time are derived and presented in the middle panel of Figure 9. The bottom panel shows time series of the satellite-derived disturbance ΔH for various dipole Local Times as well as the *Dst*-index (for this comparison with satellite data a 20 nT offset correction has been added to *Dst*).

The first hours of the time series shown in the figure reveal geomagnetic quiet conditions, but on 10 May, just before 11 UT, a Sudden Storm Commencement (ssc), characterised by a sudden *increase* in the *Dst*-index and the horizontal magnetic field component ΔH at the equator, indicates the beginning of the storm. This increase in ΔH is, however, only observed on the dayside, as expected for a compression of the magnetopause during an ssc and witnessed by the yellow colour for T_d between 06 and 18. The following *decrease* of ΔH indicates the beginning of the main phase of the storm; also this part does not start simultaneously at all longitudes but has its beginning around local midnight and moves towards all LT sectors within a few hours. The minimum value of ΔH occurs in the morning hours of 11 May 2024; when averaging over all longitudes, the satellite-derived value of about −450 nT is slightly larger than that seen in *Dst* (−412 nT). However, there is strong asymmetry regarding Local Time, with the values during dusk being about 150 nT more negative than those during dawn.

The recovery phase of the storm is shortest in the evening sector but lasts longer (until late afternoon on 11 May) in the morning sector. Also the subsequent weaker storms on 16 and 17 May reveal a significant Local Time dependence, with the strongest magnetic field depletion around dawn, as seen in the bottom panel of Figure 9.

For the investigations presented here, I assume that ionospheric contributions are negligible compared to those from the magnetosphere, which is likely a valid assumption for strong geomagnetic storms at non-polar latitudes. Combining satellite and ground-based magnetic data allows for separating magnetospheric, ionospheric and ground-induced parts, as has been done, e.g. in the Comprehensive Model Series (e.g., Sabaka et al., 2020). Following the decomposition approach developed by Min JT and Grayver (2025), a thorough investigation of the time–space structure of the May 2024 storm by combining available ground observatory and satellite magnetic data, including *Swarm* and MSS-1, is currently under investigation.

5. Summary and Conclusions

This article investigates the combination of magnetic data from the MSS-1 and *Swarm* satellites for improved investigations of Earth's magnetic field and Geospace. The study describes the complementary nature of polar-orbiting (*Swarm*) and low-inclination (MSS-1) satellites in geomagnetic field modelling and for monitoring large-scale magnetospheric contributions.

Combining MSS-1's low-inclination data with *Swarm*'s near-polar observations significantly enhances the spatial–temporal resolution of Earth's magnetic field models, allowing for new opportunities for studying both rapid core field variations at low latitudes and the local-time dependence of large-scale magnetospheric current systems.

The results presented here use MSS-1 as an example of a low-inclination satellite. While MSS-1 is an important step toward a more complete global geomagnetic observing system, there are additional exciting advances on the horizon with the NanoMagSat mission (Hulot et al., 2018) consisting of one near-polar and two low-inclination ($i = 60°$) satellites. NanoMagSat is in the pipeline as an ESA Scout mission for launch within the next few years, and many of the findings presented here using MSS-1 are also relevant for other low-inclination satellites such as NanoMagSat.

Acknowledgments

I am grateful to the European Space Agency (ESA) for operating the *Swarm* satellite trio and to the China National Space Administration (CNSA) and the Macau Foundation for operating the MSS-1 satellite. Constructive comments from two anonymous reviewers helped to improve the manuscript. This work has been carried out as part of ESA's *Swarm* DISC activities, funded by ESA contract no. 4000109587.

References

Finlay, C. C., Kloss, C., Olsen, N., Hammer, M. D., Tøffner-Clausen, L., Grayver, A., and Kuvshinov, A. (2020). The CHAOS-7 geomagnetic field model and observed changes in the South Atlantic Anomaly. *Earth Planets Space*, *72*(1), 156. https://doi.org/10.1186/s40623-020-01252-9

Gonzalez-Esparza, J. A., Sanchez-Garcia, E., Sergeeva, M., Corona-Romero, P., Gonzalez-Mendez, L. X., Valdes-Galicia, J. F., Aguilar-Rodriguez, E., Rodriguez-Martinez, M., Ramirez-Pacheco, C., ... Hernandez-Quintero, E. (2024). The Mother's Day geomagnetic storm on 10 May 2024: Aurora observations and low latitude space weather effects in Mexico. *Space Wea.*, *22*(11), e2024SW004111. https://doi.org/10.1029/2024sw004111

Hammer, M. D., Cox, G. A., Brown, W. J., Beggan, C. D., and Finlay, C. C. (2021). Geomagnetic Virtual Observatories: monitoring geomagnetic secular variation with the Swarm satellites. *Earth Planets Space*, *73*(1), 54. https://doi.org/10.1186/s40623-021-01357-9

Hayakawa, H., Ebihara, Y., Mishev, A., Koldobskiy, S., Kusano, K., Bechet, S., Yashiro, S., Iwai, K., Shinbori, A., ... Miyoshi, Y. (2025). The solar and geomagnetic storms in 2024 May: A flash data report. *Astrophys. J.*, *979*(1), 49. https://doi.org/10.3847/1538-4357/ad9335

Hulot, G., Sabaka, T. J., Olsen, N., and Fournier, A. (2015). The present and future geomagnetic field. In G. Schubert (Ed.), *Treatise on Geophysics* (2nd ed, Vol. 5, pp. 33–78). Oxford: Elsevier. https://doi.org/10.1016/B978-0-444-53802-4.00096-8

Hulot, G., Léger, J. M., Vigneron, P., Jager, T., Bertrand, F., Coïsson, P., Deram, P., Boness, A., Tomasini, L., and Faure, B. (2018). Nanosatellite high-precision magnetic missions enabled by advances in a stand-alone scalar/vector absolute magnetometer. In *IGARSS 2018-2018 IEEE International Geoscience and Remote Sensing Symposium* (pp. 6320–6323). Valencia, Spain: IEEE. https://doi.org/10.1109/IGARSS.2018.8517754

Kwak, Y. S., Kim, J. H., Kim, S., Miyashita, Y., Yang, T., Park, S. H., Lim, E. K., Jung, J., Kam, H., ... Talha, M. (2024). Observational overview of the May 2024 G5-

level geomagnetic storm: from solar eruptions to terrestrial consequences. *J. Astron. Space Sci.*, *41*(3), 171–194. https://doi.org/10.5140/jass.2024.41.3.171

Mandea, M., and Olsen, N. (2006). A new approach to directly determine the secular variation from magnetic satellite observations. *Geophys. Res. Lett.*, *33*(15), L15306. https://doi.org/10.1029/2006GL026616

Min, J. T., and Grayver, A. (2025). A decade of the fast-varying ionospheric and magnetospheric magnetic fields. *Geophys. J. Int.*. https://doi.org/10.1093/gji/ggaf065

Olsen, N. (2002). A model of the geomagnetic field and its secular variation for epoch 2000 estimated from Ørsted data. *Geophys. J. Int.*, *149*(2), 454–462. https://doi.org/10.1046/j.1365-246X.2002.01657.x

Olsen, N., and Kotsiaros, S. (2011). Magnetic satellite missions and data. In M. Mandea, et al. (Eds.), *Geomagnetic Observations and Models* (Vol. 5, pp. 27–44). Dordrecht: Springer. https://doi.org/10.1007/978-90-481-9858-0_2

Olsen, N., Lühr, H., Finlay, C. C., Sabaka, T. J., Michaelis, I., Rauberg, J., and Tøffner-Clausen, L. (2014). The CHAOS-4 geomagnetic field model. *Geophys. J. Int.*, *197*(2), 815–827. https://doi.org/10.1093/gji/ggu033

Olsen, N., and Floberghagen, R. (2018). Exploring Geospace from space: the Swarm satellite constellation mission. *Space Res. Today*, *203*, 61–71. https://doi.org/10.1016/j.srt.2018.11.017

Olsen, N., Albini, G., Bouffard, J., Parrinello, T., and Tøffner-Clausen, L. (2020). Magnetic observations from CryoSat-2: calibration and processing of satellite platform magnetometer data. *Earth Planets Space*, *72*(1), 48. https://doi.org/10.1186/s40623-020-01171-9

Olsen, N. (2022). Modelling Earth's lithospheric magnetic field using satellites in low-perigee elliptical orbits. *Geophys. J. Int.*, *232*(3), 2035–2048. https://doi.org/10.1093/gji/ggac422

Sabaka, T. J., Tøffner-Clausen, L., Olsen, N., and Finlay, C. C. (2020). CM6: a comprehensive geomagnetic field model derived from both CHAMP and Swarm satellite observations. *Earth Planets Space*, *72*(1), 80. https://doi.org/10.1186/s40623-020-01210-5

Stolle, C., Michaelis, I., Xiong, C., Rother, M., Usbeck, T., Yamazaki, Y., Rauberg, J., and Styp-Rekowski, K. (2021). Observing Earth's magnetic environment with the GRACE-FO mission. *Earth Planets Space*, *73*(1), 51. https://doi.org/10.1186/s40623-021-01364-w

Yang, Y. Y., Zhou, B., Hulot, G., Olsen, N., Wu, Y. Y., Xiong, C., Stolle, C., Zhima, Z., Huang, J. P., ... Shen, X. H. (2021). CSES high precision magnetometer data products and example study of an intense geomagnetic storm. *J. Geophys. Res.: Space Phys.*, *126*(4), e2020JA028026. https://doi.org/10.1029/2020ja028026

Zhang, K. (2023). A novel geomagnetic satellite constellation: Science and applications. *Earth Planet. Phys.*, *7*(1), 4–21. https://doi.org/10.26464/epp2023019